Mathematical modelling of cold start effects over zeolite SCR catalysts for exhaust gas aftertreatment

Massimo Colombo[a], Isabella Nova[a], Enrico Tronconi[a,*], Volker Schmeiβer[b], Michel Weibel[b]

[a] *Dipartimento di Energia, Laboratory of Catalysis and Catalytic Processes, Politecnico di Milano, Piazza Leonardo da Vinci 32, I-20133, Milano, Italy*
[b] *Daimler AG, HPC G206, 70546 Stuttgart, Germany*

Received 17 November 2013
Received in revised form 30 January 2014
Accepted 31 January 2014
Available online 4 March 2014

1. Introduction

The control of NO_x and particulate matter (PM) emissions from diesel vehicles and the fulfilment of new governmental legislations is still a challenge in the automotive field [1]. The control of PM emissions is mainly based on the application of diesel particulate filters (DPF). On the other hand, NH_3/urea SCR is the most widely used technology for the abatement of NO_x [1]. The state-of-the-art in the SCR field is associated with the application of Fe- or Cu-exchanged zeolites, showing high and stable NO_x conversions over a wide temperature range. The SCR performance as well as the continuous soot oxidation on the filter benefit from an increased NO_2/NO_x-ratio in the exhaust gas, so that a diesel oxidation catalyst is placed upstream of the filter and of the SCR converter. As a consequence, a modern common diesel vehicle aftertreatment system consists of the following devices: diesel oxidation catalyst, particle filter, AdBlue® injection and SCR catalyst, possibly followed by an NH_3 slip catalyst (ASC) [1].

Design and optimization of aftertreatment systems is a complex, challenging and expensive task, dealing with topics like temperature and AdBlue® dosing strategy for minimal emissions at reasonable costs. Such a complex target justifies the development and the application of simulation tools to reduce costs and efforts, as successfully done over many years by several research groups. The "standard" SCR reaction ($2NH_3 + 2NO + ½O_2 \rightarrow 2N_2 + 3H_2O$), and more recently the other reactions occurring when NO_2 is also present in the exhausts, have been analysed in details in the last decade [2–5], with the "Fast" ($2NH_3 + NO + NO_2 \rightarrow 2N_2 + 3H_2O$) and "$NO_2$" ($8NH_3 + 6NO_2 \rightarrow 7N_2 + 12H_2O$) SCR reactions significantly contributing to the overall $DeNO_x$ process. The overall NH_3–NO–NO_2–O_2 SCR chemistry is well understood in the temperature range of common SCR operation starting from ca. 150 °C up to 600 °C. For this reason the SCR performance can be successfully predicted by simulation tools in this temperature window. On the contrary, SCR reactions at lower temperatures are often neglected in simulations for two main reasons: i) it is assumed that NO_2 is not yet produced over the DOC, ii) NH_3 is not available in significant amounts at the SCR because AdBlue® injection and processing require a certain temperature level, typically above 150–170 °C, for complete urea decomposition/hydrolysis. However, the behaviour of SCR converters below 150 °C is becoming more and more important, because of the continuous decrease of the average exhaust temperatures with increasing fuel efficiency of the engine, and mostly because of the large contribution to overall NO_x emissions associated with the cold start transient.

Indeed, several phenomena occur at low temperatures (<150 °C) which should not be neglected. From engine test bench experiments with real exhaust gas it was observed that during the first

* Corresponding author. Tel.: +39 02 2399 3264; fax: +39 02 2399 3318.
E-mail address: enrico.tronconi@polimi.it (E. Tronconi).

Table 1
Reactions of the detailed kinetic model.

Reaction no.	Reaction name	
1	NH_3 adsorption/desorption	$NH_3 \leftarrow\rightarrow NH_3{}^*$
2	NO_2 adsorption desorption	$2\ NO_2 + 2\ S\text{-}OH \leftarrow\rightarrow S\text{-}ONO + S\text{-}NO_3 + H_2O$
3	Nitrite oxidation to nitrates	$NO_2 + S\text{-}ONO \leftarrow\rightarrow NO + S\text{-}NO_3$
4	Nitrates thermal decomposition	$S\text{–}NO_3 + 1/2\ H_2O \rightarrow NO_2 + 1/4\ O_2 + S\text{–}OH$
5	Nitrites reduction by NH_3	$S\text{–}ONO + NH_3{}^* \rightarrow N_2 + H_2O + S\text{–}OH$
6	Nitrates reduction by NH_3	$S\text{–}NO_3 + 2/3\ NH_3{}^* \rightarrow S\text{–}ONO + 1/3\ N_2 + H_2O$
7	Blocking of nitrates by NH3	$S\text{–}NO_3 + NH_3{}^* \leftarrow\rightarrow S\text{-}NO_3[NH_3]$
8	Ammonia–nitrates complex decomposition to N_2O	$S\text{–}NO_3[NH_3] \rightarrow N_2O + H_2O + S\text{–}OH$
9	NH_4NO_3 formation	$2\ NH_3{}^* + 2\ NO_2 \rightarrow NH_4NO_3{}^* + N_2 + H_2O$
10	NH_4NO_3 sublimation	$NH_4NO_3{}^* \rightarrow [NH_3 + HNO_3] \rightarrow NH_4NO_3$
11	NH_4NO_3 thermal decomposition to N_2O	$NH_4NO_3{}^* \rightarrow N_2O + 2\ H_2O$
12	NO oxidation	$NO + 1/2\ O_2 \leftarrow\rightarrow NO_2$
13	Slow-SCR	$3/2\ NO + NH_3{}^* \rightarrow 5/4\ N_2 + 3/2\ H_2O$

seconds after cold start NO_x emissions are completely absent after the SCR brick [6]. Moreover, after a while the exhaust gas leaving the SCR shows a significantly higher temperature than the gas entering the catalyst. When the temperature rise is at its maximum, a NO_x emission peak can be measured, followed by a slow decrease in gas temperature after the SCR catalyst.

In a previous contribution [6], such effects, playing a major role in the cold start behaviour of SCR converters, have been investigated experimentally over a commercial monolith Cu-zeolite SCR catalyst. All the effects were reproduced successfully both at the lab scale and at the engine test bench. A significant NO oxidation activity was observed over the investigated commercial Cu-zeolite at temperatures below 100 °C, as long as the exhaust gas was dry, a condition verified during the initial cold start transient due to H_2O condensation on aftertreatment devices upstream the SCR unit. The NO oxidation activity exhibited a negative temperature dependence [7] and was suppressed in the presence of H_2O. The produced NO_2 was efficiently adsorbed on the SCR catalyst, so that no end of pipe NO_x was observed after cold start for some minutes. When H_2O in the exhausts eventually reached the SCR catalyst, adsorption and condensation occurred in the zeolite pores. This resulted in gas and monolith heat up so that a strong temperature rise occurred. Such a temperature increase was identified as responsible for the desorption of previously stored NO_x.

In this contribution a mathematical model of the cold start process is developed and appended to an existing simulation model of SCR converters [8]. We start from a microkinetic model recently published by our group that describes the NO_2 related SCR reactions for $T > 100$ °C on the basis of a complex reaction network accounting for NO_2 storage with formation of nitrites and nitrates, and for their reactivity with NO and NH_3. In order to reproduce the cold start effects observed below 100 °C, herein we add to the kinetic scheme also the description of the low-T NO oxidation to NO_2, of NO_2 physisorption and of H_2O adsorption/desorption, namely the three steps identified in [6] as responsible for all the observed material and thermal cold start effects.

2. Methods

2.1. Experimental

Core drilled monolith samples (around 6 cm^3 in volume, 400 cpsi cell density, 5 mils) were obtained from a commercial Cu-zeolite catalyst provided by an unnamed supplier. Prior to catalytic tests, each sample was conditioned at 550 °C for 5 h in high O_2 and H_2O feed contents (10% v/v) with a GHSV of 81,000 h^{-1}. Gas phase concentrations in the range 0–8% H_2O, 0–8% O_2, 0–500 ppm of NO or NO_2 were typically fed to the reactor inlet. N_2 was used as balance gas. The space velocity was set between 100,000 h^{-1} and 30,000 h^{-1}, the latter value representing a tradeoff between real idling conditions at the engine start up and lab rig constraints. The gas temperature was monitored by a K-type thermocouple placed in the central channel of the core monolith samples. The axial location of the thermocouple tip varied in different experiments. Considering a dimensionless axial coordinate ranging from 0 to 1, the value 0 was assigned to the monolith inlet section, while the value 1 was associated to the outlet section. Where not specified, the thermocouple was located in the axial central position of the core samples (dimensionless axial coordinate = 0.5). To achieve an efficient temperature control working in the low temperature region (below 100 °C), the reactor and the inlet lines were not heated during the experiments, except the feed line of H_2O, which needed to be vaporized. On the contrary, outlet lines were heated to prevent products condensation. Gas phase analysis was performed using an UV-analyzer (ABB LIMAS 11HV) for the analysis of NO, NO_2, NH_3 and a Non Dispersive IR Analyzer (ABB Uras-14) for the analysis of N_2O. A more detailed description of the experimental rig is provided in [9,10].

2.2. Modeling

The dual site detailed kinetic scheme of Colombo et al. [8] has been used as starting point for the development of the cold start model. Such a kinetic scheme is based on the reaction steps and rate equations listed in Table 1 and Table 2, respectively.

The mechanism accounts for NH_3 adsorption and desorption onto acidic sites, whose coverage is identified by the symbol theta.

Table 2
Rate equations adopted for the detailed kinetic model.

Rate	Rate equation
r1	$r_1 = k_{1_{ADS}} \cdot C_{NH_3} \cdot \vartheta_{free} - k_{1_{DES}} \cdot \vartheta_{NH_3}$ $k_{1_{DES}} = \exp\left\{\beta_{1_{DES}} - \gamma_{1_{DES}} \cdot \left[\frac{1000\left(1-\alpha\cdot(\vartheta_{NH_3}+\vartheta_{NH_4NO_3}\right)}{T} - \frac{1000}{T_{REF}}\right]\right\}$
r2	$r_2 = k_{2_{DIR}} \cdot \left(C_{NO_2} \cdot \sigma_{free}\right)^2 - k_{2_{INV}} \cdot \sigma_{ONO} \cdot \sigma_{NO_3}$
r3	$r_3 = k_{3_{DIR}} \cdot C_{NO_2} \cdot \sigma_{ONO} - k_{3_{INV}} \cdot C_{NO} \cdot \sigma_{NO_3}$
r4	$r_4 = k_4 \cdot \sigma_{NO_3}$
r5	$r_5 = k_5 \cdot \vartheta_{NH_3} \cdot \sigma_{ONO}$
r6	$r_6 = k_6 \cdot \sigma_{NO_3} \cdot \vartheta_{NH_3}$
r7	$r_7 = k_{7_{DIR}} \cdot \vartheta_{NH_3} \cdot \sigma_{NO_3} - k_{7_{INV}} \cdot \sigma_{NO_3[NH_3]}$
r8	$r_8 = k_8 \cdot \sigma_{NO_3[NH_3]}$
r9	$r_9 = \frac{k_9 \cdot \vartheta_{NH_3} \cdot C_{NO_2}^2}{1+K_{Amm} \cdot \vartheta_{NH_4NO_3}}$
r10	$r_{10} = k_{10} \cdot \vartheta_{NH_4NO_3}$
r11	$r_{11} = k_{11} \cdot \vartheta_{NH_4NO_3}$
r12	$r_{12} = k_{12} \cdot \left[C_{NO} \cdot \left(P_{O_2}\right)^{0.5} - \frac{C_{NO_2}}{K_{EQ_{NO}}}\right] \cdot \left\{\frac{P_{H_2O}}{0.03}\right\}^{\vartheta}$ $K_{EQ_{NO}} = \exp\left[-\frac{(-13804+18.238\cdot T)}{RT}\right]$
r13	$r_{13} = k_{13} \cdot \vartheta_{NH_3} \cdot C_{NO}$

Note: where not specified $k_j = \exp\left\{\beta_j - \gamma_j \cdot \left[\frac{1000}{T} - \frac{1000}{T_{REF}}\right]\right\}$, $T_{ref} = 473$ K

Table 3
Additional reactions to account for cold start effects.

Reaction no.	Reaction name	
14	H_2O Adsorption/desorption	$H_2O \leftarrow\rightarrow H_2O^{ads}$
15	Low temperature NO oxidation	$NO + ½\ O_2 \rightarrow NO_2$
16	NO_2 physisorption	$NO_2 \leftarrow\rightarrow NO_2^{ads}$

On the contrary, steps (2)–(8), involving nitrites/nitrates formation and reactivity, are assumed to proceed on "S-sites", associated with the Cu promoter of the zeolite catalyst, whose coverage is identified by the symbol sigma. The same mechanism includes also a few more global reactions, namely the reversible NO oxidation to NO_2 (12), the Slow-SCR (13) reaction and the ammonium nitrate formation, sublimation and decomposition to N_2O (9-11).

To account for cold start effects ($T < 150\,^{\circ}C$), three additional reactions and the related rate equations were added to the above kinetic scheme, consistently with the phenomena identified in [6] (see Tables 3 and 4).

The two kinetic schemes above were incorporated into the transient 1D + 1D mathematical model of honeycomb SCR catalytic reactors described by Chatterjee et al. [11–13]. The model assumes identical conditions within each channel of the monolith catalyst, with negligible axial dispersion and pressure drop. External (gas–solid) mass transfer, described by well-established correlations for mass transfer coefficients, as well as intra-phase diffusional limitations, accounted for by equations for diffusion–reaction of the gaseous species in the catalytic washcoat, are both considered in the model. The effective diffusivities are evaluated from the catalyst morphology according to a modified Wakao–Smith model [14].

3. Results and discussion

3.1. Water adsorption–desorption

It was shown in [6] that when H_2O in the exhaust gas reached the SCR catalysts, it condensed onto the zeolite where it was adsorbed as well. These phenomena were associated with a strong temperature rise of both the solid and the gas phase, due to the high heat of condensation of H_2O in the zeolite pores. The exothermal effect was significant and the SCR outlet temperature could even exceed the inlet gas temperature.

Fig. 1A shows experimental data for a water adsorption test carried out at 45 °C feeding 8% v/v H_2O at a space velocity of 100,000 h^{-1}. The test was repeated three times changing the axial position of the thermocouple inside the monolith channel. Considering a dimensionless axial coordinate ranging from 0 to 1, the value 0 was assigned to the monolith inlet section, while the value 1 was associated to the outlet section. It can be seen that independently

Table 4
Rate equations for the additional reactions.

Rate	Rate equation
r14	$r_{14} = r_{14_{ADS}} - r_{14_{DES}}$ $r_{14_{Ads}} = k_{14-ADS} \cdot P_{H_2O} \cdot \vartheta_{free}$ $r_{14_{Des}} = k_{14-Des} \cdot \vartheta_{H_2O}$ $k_{Des} = \exp\left\{k^0_{Des} - E_{Des} \cdot \left[\frac{1000}{T} - \frac{1000}{T_{REF}}\right]\right\}, \quad T_{ref} = 473K$
r15	$r_{15} = k_{15} \cdot \frac{c_{NO} \cdot P_{O_2}}{\left(1 + K_{NOP} \cdot P_{H_2O}\right)}$ $k_{15} = \exp\left\{k^0_{15} - E_{15} \cdot \left[\frac{1000}{T} - \frac{1000}{T_{REF}}\right]\right\}, T_{ref} = 298K$
r16	$r_{16} = r_{16_{ADS}} - r_{16_{DES}}$ $r_{16_{Ads}} = k_{16_{ADS}} \cdot C_{NO_2} \cdot \vartheta_{free}$ $r_{16_{Des}} = k_{16_{Des}} \cdot \vartheta_{NO_2}$ $k_{16Des} = \exp\left\{k^0_{16Des} - E_{16Des} \cdot \left[\frac{1000}{T} - \frac{1000}{T_{REF}}\right]\right\}, T_{ref} = 298K$

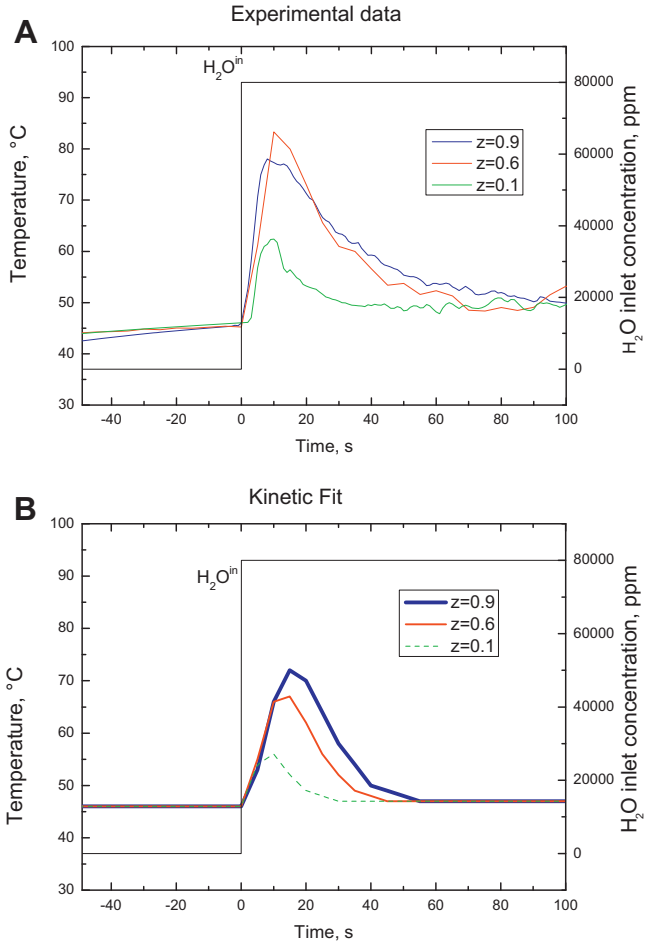

Fig. 1. Temperature behaviour inside the monolith channel at different axial locations upon addition of H_2O to the gas feed. H_2O = 8% v/v; GHSV = 100,000 h^{-1}; Adsorption temperature = 45 °C. A) Experimental data; B) Kinetic fit.

from the axial location of the thermocouple, upon addition of H_2O at $t = 0$ s a temperature rise was observed. However, depending on the axial location, the magnitude of the phenomenon was different, being more significant at the monolith outlet.

The thin lines in Fig. 2 represents the experimental data of a water adsorption/desorption test performed at 60 °C with a space

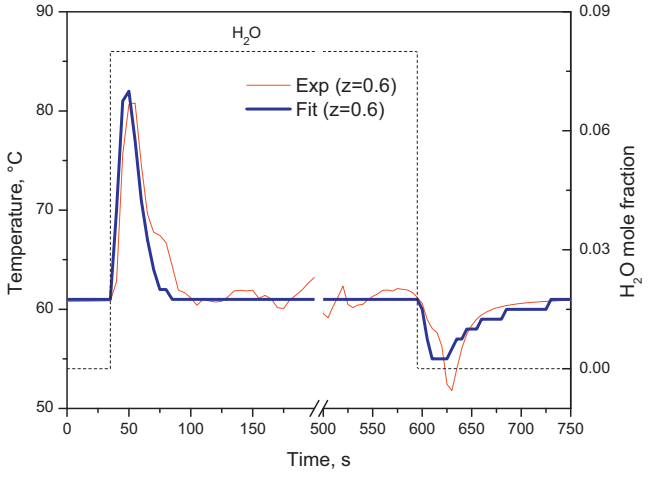

Fig. 2. Temperature behaviour inside the monolith channel upon addition and shut off of H_2O to the gas feed. H_2O = 8% v/v; GHSV = 100,000 h^{-1}; Adsorption temperature = 60 °C. Thin lines: experimental data; thick lines: model fit.

velocity of 100,000 h^{-1} and a water feed concentration of 8% v/v. The same qualitative trend described for Fig. 1A was observed at H_2O feed, with a temperature rise of about 20 °C after water feed (t = 35 s). After H_2O shut off, at t = 600 s a temperature drop occurred, with a temperature difference of about 10 °C, in line with what reported in [6].

Notably, upon feeding H_2O, after the transient thermal effect related to water condensation, the same temperature initially observed when feeding only dry gases was restored. This indicates that the enthalpy contribution resulting from addition of water vapour to the feed stream was essentially negligible.

The kinetic parameters of the H_2O adsorption/desorption rate (r_{14}) were estimated by fitting the data in Fig. 1A and Fig. 2, while the storage capacity of the same species was determined from porosity analysis, assuming that water can fill the entire volume of the zeolite pores. Fig. 1B and the thick line in Fig. 2 show the fit results. A fairly good overall qualitative and quantitative agreement with experimental data can be noted. The model is able to reproduce the phenomena observed at both water feed and shut-off, as well as the temperature profile recorded at different axial locations along the monolith channel.

3.2. NO oxidation

The second step contributing to the cold-start phenomena identified in [6] was the NO oxidation to NO_2 occurring at temperatures below 100 °C. As reported in [6], the investigated commercial Cu-zeolite SCR exhibited a significant NO oxidation activity at such temperatures in dry exhausts. Notably, such NO oxidation activity exhibited a negative temperature dependence going from room temperature up to 100 °C. The kinetics were first order in oxygen concentration, and were strongly inhibited by the presence of water (r.15).

Figs. 3–5, thin lines, show the transient behaviour and steady state NO conversion during three NO oxidation tests performed in the temperature range 25–550 °C feeding 500 ppm of NO at a space velocity of 100,000 h^{-1}. Fig. 3 shows experimental results collected in a dry stream with 8% v/v O_2 at reactor inlet; Fig. 4 shows results obtained reducing the feed oxygen content to 2% v/v, and Fig. 5 shows results obtained with a wet stream containing 8% v/v of both H_2O and O_2.

Looking at the thin lines in Fig. 3A it can be seen that, upon feeding O_2 at t = 5650 s, immediate NO conversion was observed, while a dead time was shown by the NO_2 signal. The NO trace rapidly reached a steady state value of about 400 ppm, while the NO_2 concentration started increasing about 1000 s after O_2 feed and slowly approached a steady state level of about 100 ppm. Such a trend can be explained considering the oxidation of NO to NO_2, occurring at low temperatures, and the following storage of NO_2 in the form of surface nitrates [2,4,8,15,16] and physisorbed NO_2 until catalyst saturation. The increase of the catalyst temperature resulted in the progressive decrease of NO conversion at temperatures up to 150 °C. It has to be noticed that each time the catalyst temperature was increased, NO_2 desorption occurred, indicating the presence of weakly bonded NO_2 species. Such NO_2 desorption cannot be related to the decomposition of surface nitrates species, which are stable on the same catalyst at temperatures as high as 230 °C [8]. The further increase of the catalyst temperature from 150 °C to 550 °C in a ramp at 20 °C/min resulted eventually in the onset of the "high temperature" NO oxidation, as evidenced by a growing consumption of NO in the 150–400 °C temperature range and the subsequent decrease related to the approach of thermodynamic equilibrium conditions. During the temperature ramp desorption of previously adsorbed nitrates species also occurred, as evidenced by the nitrogen balance.

The same qualitative trend was observed decreasing the O_2 content to 2% v/v (Fig. 4A). In this case a lower NO consumption rate

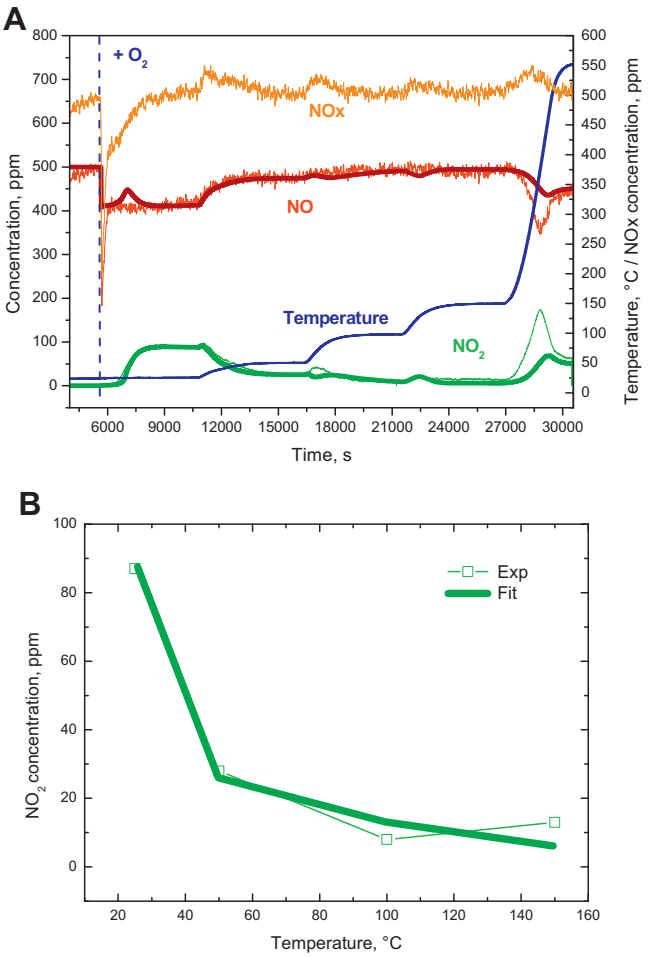

Fig. 3. NO oxidation at low temperature. NO = 500 ppm; H_2O = 0% v/v; O_2 = 8% v/v; GHSV = 100,000 h^{-1}. A) Transient behavior. B) Steady state NO_2 concentration as a function of temperature. Thin lines: experimental data; thick lines: model fit.

resulted in a slower saturation of the catalyst surface, as indicated by the longer dead time in the NO_2 trace and the slow approach to steady state conditions at ambient temperature. On the contrary, the presence of water completely suppressed the NO oxidation activity below 150 °C, as shown in Fig. 5.

The presented data were used to estimate the rate parameters for the low temperature NO oxidation reaction (r15) and for NO_2 physisorption (r16). The thick lines in Figs. 3–5 represent the kinetic fit results. A very good correlation between experimental data and model fit can be observed both in terms of steady state NO conversions and most notably in terms of transient behaviour. Only in Fig. 3A the model showed a transient behaviour not displayed by the experimental data. Indeed, around t = 7000 s, the computed NO signal showed a maximum before reaching steady state. Such a transient behaviour is associated with the storage of NO_2 as nitrates according to reactions 2 and 3. Although such storage is likely to occur experimentally, as indicated by NO_x release at high temperatures, the rate of reaction (3) at room temperature seems to be slightly overestimated, resulting in the onset of a small NO peak.

3.3. Reproduction of overall cold start transient

In [6] it was shown that a suitable sequence of NO oxidation to NO_2, NO_2 adsorption/desorption and H_2O adsorption steps could qualitatively reproduce at the lab scale the cold start phenomena

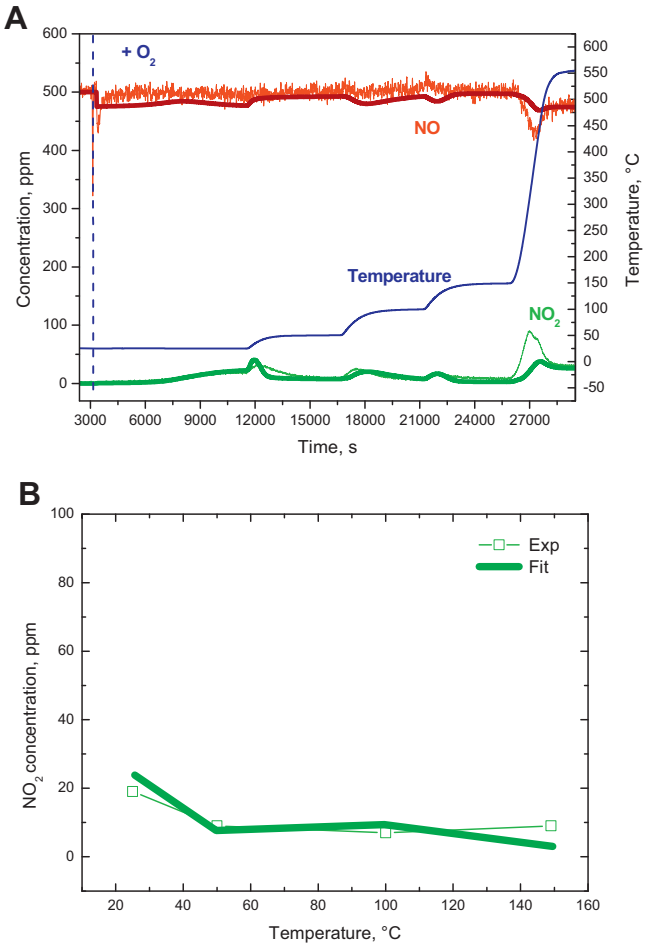

Fig. 4. NO oxidation at low temperature. Effect of oxygen concentration. NO = 500 ppm; H_2O = 0% v/v; O_2 = 2% v/v; GHSV = 100,000 h^{-1}. A) Transient behavior. B) Steady state NO_2 concentration as a function of temperature. Thin lines: experimental data; thick lines: model fit.

observed in engine test bench experiments with real exhaust gas. For this purpose 500 ppm of NO in 8% O_2 and N_2 as balance gas were fed to the test reactor, loaded with a Cu-zeolite SCR catalyst, during a transient in which 0–8% of H_2O was pulsed at room temperature. Results from such an experiment are shown in Fig. 6. NO was immediately converted as soon as O_2 was introduced in the reactor at t = 7400 s, with the NO_2 signal showing a dead time, due to its adsorption on the catalyst. When H_2O was introduced in the reactor, an increase in temperature associated with a peak of NO_2 in the gas phase was observed, thus qualitatively reproducing what was observed at the test bench scale.

After estimating the rate parameters for the low temperature NO oxidation to NO_2, NO_2 adsorption/desorption and H_2O adsorption, the resulting kinetic scheme comprising all reactions from r1 to r16 was used to perform a predictive simulation of the test discussed above. The thick lines in Fig. 6 represent the simulation results: it is apparent that the model herein derived is able to qualitatively describe the observed trends, from NO conversion upon O_2 feed to the increase of gas phase temperature associated with NO_2 release at H_2O feed. A reasonable match between predictive simulations and experimental data can also be observed from the quantitative point of view, thus providing evidence that the developed kinetic scheme is able to describe phenomena responsible for the cold start effects observed at the engine test bench scale.

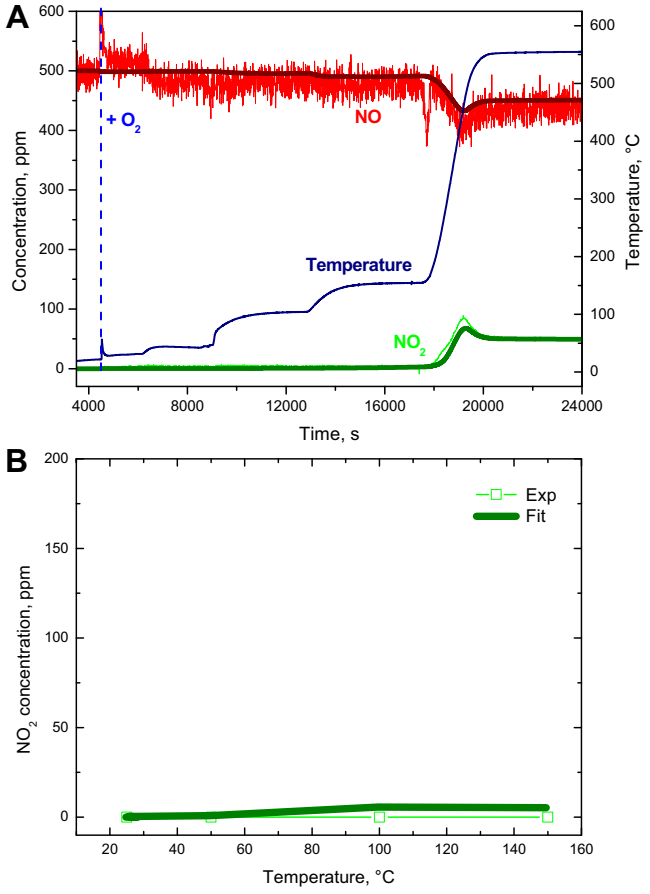

Fig. 5. NO oxidation at low temperature. Effect of water. NO = 500 ppm; H_2O = 8% v/v; O_2 = 8% v/v; GHSV = 100,000 h^{-1}. A) Transient behavior. B) Steady-state NO_2 concentration as a function of temperature. Thin lines: experimental data; thick lines: model fit.

3.4. Predictive simulation of WHTC temperature behavior

In [6] we reported the temperature evolution of the exhaust gas measured before and after the SCR brick during a World Harmonized Transient Cycle (WHTC). While the inlet gas showed a slow but continuous rise in temperature, the gas leaving the SCR catalyst did not follow the same trend. The outlet temperature profile showed in fact a sudden rise (about 80 °C) starting at ~ 100 s after

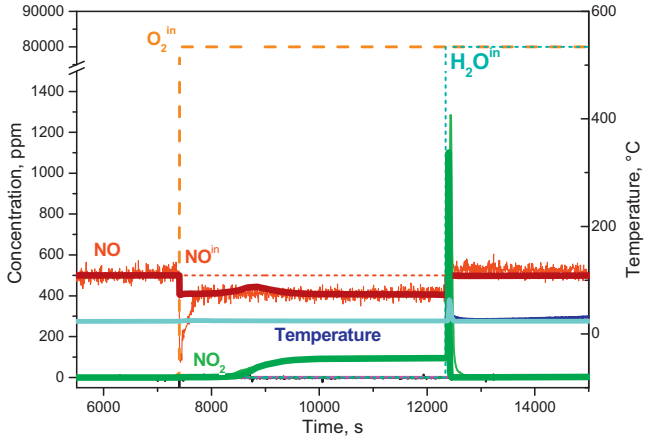

Fig. 6. Cold Start experiment, lab scale: NO = 500 ppm; O_2 = 0–8%: H_2O = 0–8%. GHSV = 30,000 h^{-1}. T = 25 °C. Thin lines: experimental data; thick lines: model simulation.

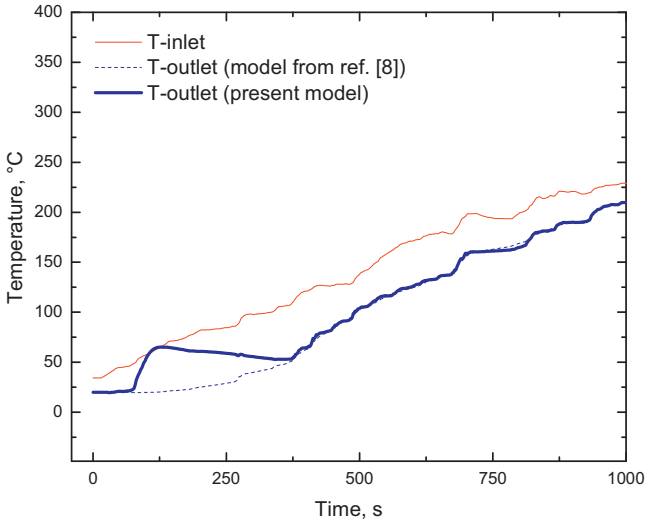

Fig. 7. Temporal evolution of the gas temperature before and after the SCR catalyst during the cold part of a World Harmonized Transient Cycle (WHTC). The outlet T-profiles are simulated using the herein developed model and, for comparison, the model taken from [8], which neglects H_2O adsorption.

start, reached its temporarily highest value at ~ 250 s (with the outlet temperature exceeding the inlet one), then it slowly decreased over the next 350 s. The temperature of the system finally rose again after 600 s, showing the conventional heat-up behavior.

In order to confirm that the herein developed model can effectively reproduce the observed thermal effects during real cold start transients, we performed a predictive simulation of a WHTC cycle. Fig. 7 compares the simulation obtained with the model developed in this contribution (thick blue line) and the corresponding simulation obtained with the kinetic model developed in [8] (dashed thin line), which does not account for the low temperature phenomena herein discussed. It can be noticed that when the adsorption/desorption of water is not taken into account, the simulated SCR outlet temperature follows closely the inlet temperature profile, in line with the convective heating of the brick by the feed gases. On the contrary, when the water adsorption/desorption is taken into account the same qualitative features observed in [6] are reproduced by the model: after about 100s the temperature suddenly increased, approaching the inlet value, then the temperature decreased slowly for about 250s before following the conventional heat-up behavior.

4. Summary/Conclusion

Following an experimental investigation of cold start effects on the material and thermal behaviour of a Cu-zeolite SCR catalyst, in this contribution a physically and chemically consistent mathematical model of the related phenomena has been developed and included into an existing SCR converter model to reproduce cold start transients in engine test bench runs.

In analogy with the approach of the previous experimental study, the three physical-chemical steps identified as responsible for the cold start effects, namely H_2O adsorption/desorption, low temperature NO oxidation to NO_2 and NO_2 physisorption, were incorporated into an existing detailed SCR kinetic model, with the new rate parameters fitted to experimental data analyzing the individual steps. The resulting simulation model successfully reproduced the features of cold start transients observed during both lab scale dedicated experiments and full-scale engine test bench runs.

References

[1] T. Johnson, Vehicular Emissions in Review, SAE Technical Paper 2012-04-16.
[2] M. Devadas, O. Kröcher, M. Elsener, A. Wokaun, N. Söger, M. Pfeifer, Y. Demel, L. Mussmann, Influence of NO_2 on the selective catalytic reduction of NO with ammonia over Fe-ZSM5, Appl Catal, B 67 (3–4) (2006) 187–196.
[3] A. Grossale, I. Nova, E. Tronconi, Study of a Fe-zeolite-based system as NH_3-SCR catalyst for diesel exhaust aftertreatment, Catal Today 136 (1–2) (2008) 18–27.
[4] M. Koebel, G. Madia, M. Elsener, Selective catalytic reduction of NO and NO_2 at low temperatures, Catal Today 73 (3–4) (2002) 239–247.
[5] H. Sjövall, L. Olsson, E. Fridell, R.J. Blint, Selective catalytic reduction of NO_x with NH_3 over Cu-ZSM-5—The effect of changing the gas composition, Appl Catal, B 64 (3–4) (2006) 180–188.
[6] V. Schmeisser, M. Weibel, L. Sebastian Hernando, I. Nova, E. Tronconi, M.P. Ruggeri, Cold Start Effect Phenomena over Zeolite SCR Catalysts for Exhaust Gas Aftertreatment, SAE Technical Paper 2013-01-1064.
[7] N. Artioli, R.F. Lobo, E. Iglesia, Catalysis by confinement: enthalpic stabilization of NO oxidation transition states by microporous and mesoporous siliceous materials, The J Phys Chem C 117 (40) (2013) 20666–20674.
[8] M. Colombo, I. Nova, E. Tronconi, Detailed kinetic modeling of the NH_3–NO/NO_2 SCR reactions over a commercial Cu-zeolite catalyst for diesel exhausts after treatment, Catal Today 197 (1) (2012) 243–255.
[9] M. Colombo, I. Nova, E. Tronconi, A comparative study of the NH_3-SCR reactions over a Cu-zeolite and a Fe-zeolite catalyst, Catal Today 151 (3–4) (2010) 223–230.
[10] P. Forzatti, I. Nova, E. Tronconi, A. Kustov, J.R. Thøgersen, Effect of operating variables on the enhanced SCR reaction over a commercial V_2O_5–WO_3/TiO_2 catalyst for stationary applications, Catal Today 184 (1) (2012) 153–159.
[11] D. Chatterjee, T. Burkhardt, B. Bandl-Konrad, T. Braun, E Tronconi, I Nova, C Ciardelli, Numerical Simulation of Ammonia SCR Catalytic Converters: Model Development and Application, SAE Technical Paper 2005-01-0965, 2005.
[12] D. Chatterjee, T. Burkhardt, M. Weibel, I. Nova, A. Grossale, E. Tronconi, Numerical Simulation of Zeolite and V-based SCR Catalytic Converters, SAE Technical Paper 2007-01-1136, 2007.
[13] D. Chatterjee, T. Burkhardt, M. Weibel, E. Tronconi, I. Nova, C. Ciardelli, Numerical Simulation of NO/NO_2/NH_3 Reactions on SCR Catalytic Converters: Model Development and Applications, SAE Technical Paper 2006-01-0468, 2006.
[14] R.S. Cunningham, C.J. Geankoplis, Effects of different structures of porous solids on diffusion of gases in the transition tegion, Ind Eng Chem Fundam 7 (4) (1968) 535–542.
[15] A. Grossale, I. Nova, E. Tronconi, Ammonia blocking of the "Fast SCR" reactivity over a commercial Fe-zeolite catalyst for diesel exhaust aftertreatment, J Catal 265 (2) (2009) 141–147.
[16] A. Grossale, I. Nova, E. Tronconi, Role of nitrate species in the "NO_2-SCR" mechanism over a commercial fe-zeolite catalyst for SCR mobile applications, Catal Lett 130 (3–4) (2009) 525–531.